The Role of Crystal Polarity in α-Amino Acid Crystals for Induced Nucleation of Ice

M. Gavish, J.-L. Wang, M. Eisenstein, M. Lahav,* L. Leiserowitz*

The hydrophobic faces of single crystals of a series of pairs of racemic and chiral-resolved hydrophobic α-amino acids were used as a substrate, onto which water vapor has been cooled to freezing. The morphologies and molecular packing arrangements within each crystal pair are similar but only one of each pair exhibits a polar axis, parallel to the hydrophobic face exposed to water. Those crystals that have a polar axis induce a freezing point higher by 4° to 5°C than the corresponding crystals that do not have a polar axis. The results are interpreted in terms of an electric field mechanism that helps align the water molecules into ice-like clusters en route to crystallization.

Heterogeneous freezing of supercooled water into ice is a widespread phenomenon. For example, the ability of a variety of cold-blooded animals to survive the winter months in polar climates is affected by the onset temperature at which freezing begins in their body fluids, which is determined to a large extent by the presence of antifreeze agents, such as polyhydroxyl alcohols and various proteins, in their blood serum (*1–3*). In more temperate zones, promotion of ice nucleation by frost bacteria (*4, 5*) can cause extensive damage to nonconiferous plants at temperatures as high as −4°C. On the positive side, such promotion has been exploited for the induction of rainfall with the assistance of crystalline silver iodide (AgI) seeded in clouds (*6*). Surprisingly, pinpointing the various mechanisms responsible for the promotion of ice nucleation on the molecular level is still a challenge, perhaps because of the complexity of the process. The proposed mechanism that has been generally accepted is that a substrate crystal promotes ice formation when there is a match between the crystal lattices of nucleator and nucleant, as exemplified by the use of the hexagonal polymorph of AgI. However, pure AgI is not an efficient ice nucleator (*7*). The crystal must contain cationic impurities such as NH_4^+ (*8*); evidence for a structural fit has been found, for example, in various complex phases of AgI with NH_4I (*9*), which contain layered water with an arrangement similar to that of hexagonal ice. The necessity for a structural match is further borne out by recent studies on induced ice nucleation from a two-dimensional surface of long-chain aliphatic alcohols arranged as monolayers on drops of water (*10*); these systems involve both a partial lattice and structural match (*11, 12*).

In a search for other possible mechanisms for the promotion of ice nucleation, we came across intriguing reports (*13–15*) that the onset temperature of ice nucleation of crystalline powders of some hydrophobic α-amino acids is close to that in the AgI ice nucleation. Crystals of several of the chiral-resolved α-amino acids, particularly Leu, Val, and Phe, induce an ice freezing point higher by about 3° to 5°C than their racemic counterparts. These results were surprising because the chiral and racemic crystal forms of these amino acids (Table 1A) resemble each other both in molecular packing arrangement (*16–18*) and in crystal morphology (*18*). Moreover, the structural mismatch between the chiral and racemic counterparts is small compared to the difference between either of them and ice. Furthermore, the cell dimensions of both systems are distinctly different from those of hexagonal ice. Thus, the induction of ice nucleation by the surfaces of these crystals cannot be attributed to epitaxy (*19*). Therefore, we undertook a comparative study of induced nucleation of ice at well-developed and crystallographically isostructural faces of racemic and chiral-resolved crystals in order to discover other aspects of induced ice nucleation.

The hydrophobic α-amino acids listed in Table 1A pack in hydrogen-bonded layers (*16, 17*). In the chiral crystals, molecules within a layer are related by translation (and pseudo-translation in some crystals) symmetry only (*18*), interlinked by van der Waals contacts between the hydrocarbon residues and by N–H···O hydrogen bonds between the zwitterionic glycine moieties ($^+H_3NCHCO_2^-$), as exemplified by L-Val in Fig. 1A. In the corresponding racemic crystals, the molecules appear in layer motifs similar to their chiral counterparts as exemplified by D,L-Val in Fig. 1B. For some of the systems, such as racemic isoleucine, the layer motif comprises molecules related by glide symmetry, but even in these cases the layer structure of the racemate is similar to that of the chiral crystal. In all of these crystal structures the molecular layers, one side of which is hydrophobic and the other hydrophilic, are linked on the hydrophilic side by N–H···O bonds to form bilayers (Fig. 1, bottom). These bilayers are generated in the chiral crystals by twofold (or pseudo-twofold) symmetry (Fig. 1A) and in racemic crystals by a center of inversion (Fig. 1B). To complete the crystal structure, the neighboring bilayers make van der Waals contact across their hydrophobic surfaces, which is achieved in the chiral systems by translation symmetry between the bilayers (Fig. 1A, bottom) and in the racemates by translation or glide symmetry (Fig. 1B, bottom). Thus the chiral crystals are polar by virtue of the (pseudo) twofold axis parallel to the plane of

Table 1. Freezing points (FP) and contact angles (α) of water on α-amino acid crystals (α-amino octanoic acid, AOA). The space groups (SG) of the amino acids listed in (**A**) exhibit a polar axis for the chiral resolved (L) compounds and nonpolar axes for the racemic (D,L) compounds. The reverse situation holds for the amino acid crystals in (**B**). More than 15 FP measurements were made for each substance on different days and different specimens. These measurements were carried on in parallel for the pairs of racemic and chiral crystals. The crystal structures of chiral-resolved and racemic Val, Leu, Ile, Met, and Norleu are listed in (*16*) in the same sequence as in (A); that of *tert*-Leu is listed in (*17*) and that of AOA in (*18*).

Amino acid	Chiral-resolved crystals			Racemic crystals		
	FP (°C)	α (°)	SG	FP (°C)	α (°)	SG
A						
Val	−5.6 ± 0.6	80	$P2_1$	−9.9 ± 0.8	80	$P2_1/c$
Leu	−5.5 ± 0.5	89	$P2_1$	−8.1 ± 0.5	89	$P\bar{1}$
Ile	−5.1 ± 0.5	91	$P2_1$	−9.8 ± 0.6	89	$P\bar{1}$
Met	−3.7 ± 0.3	80	$P2_1$	−7.2 ± 0.1	79	$P2_1/a$
Norleu	−4.1 ± 0.3	88	$C2$	−6.7 ± 0.2	88	$P2_1/a$
tert-Leu	−5.8 ± 0.6	75	$P1$	−8.6 ± 0.5	73	$P2_1/c$
AOA	−4.1 ± 0.2	89	$C2$	−7.3 ± 0.3	89	
B						
Tyr	−6.6 ± 0.3		$P2_12_12_1$	−1.1 ± 0.2		$Pna2_1$
Ala	−7.5 ± 0.6		$P2_12_12_1$	−2.6 ± 0.3		$Pna2_1$

*The x-ray diffraction photographs of racemic AOA showed pronounced diffuse scattering, indicative of molecular disorder, so that the space group could not be unambiguously assigned; indications were very strong that the crystal structure is monoclinic, centrosymmetric $P2_1/c$.

Department of Materials and Interfaces, Weizmann Institute of Science, Rehovot 76100, Israel.

*To whom correspondence should be addressed

the bilayer and the absence of another symmetry element that would negate the polarity; the racemic crystals are centrosymmetric and therefore nonpolar.

All of these amino acids crystallize from aqueous solution as (001) plates whose two crystal faces are parallel to the plane of the bilayer [for simplicity we assume that the plate face of all of the crystals is (001)]. According to contact angle measurements, these faces are hydrophobic and thus expose primarily the hydrocarbon residues. Water vapor was condensed at 0°C on these faces of crystal specimens of chiral and racemic crystal pairs. These pairs of crystals of similar thickness (about 0.1 to 0.2 mm), cross-sectional area (about 1 to 2 mm^2), and shape were simultaneously cooled down to the freezing point at a rate of 1°C/min. The onset temperatures of freezing, determined by visual observation under an optical microscope (Table 1A), show a consistent trend; the polar chiral α-amino acid crystals induce freezing of water at higher temperatures than the corresponding centrosymmetric racemates, with a difference of 3° to 5°C. This result is in keeping with observations on powders (*13–15*).

In a second set of experiments, the substrate crystals were cooled to about −15°C before water vapor deposition. The nucleated ice crystals with a hexagonal morphology and a dominant (0001) face were found to emerge from cracks in the substrate α-amino acid plates (Fig. 2A). The widths of these cracks viewed under the microscope appeared to be in the range of tens of micrometers. Not all the emerging ice crystals had their (0001) faces parallel, but they were parallel within distinct regions. Furthermore, we did not observe any pronounced orientation of the (0001) face of ice with respect to the polar axis of the α-amino acid substrate crystal. After these ice crystallites appeared, the rest of the surface plates gradually became covered by ice.

In view of these observations, we propose the following model to explain the ice nucleation on a molecular level. The structures of the plate faces of the polar and nonpolar α-amino acid crystals are depicted schematically in Fig. 2, C and D. The two faces are essentially the same in structure, exposing hydrocarbon groups. Both faces contain cracks that expose the hydrocarbon as well as the strongly hydrophilic CO_2^- and NH_3^+ groups. In Fig. 2C, the structures of the two opposite surfaces within the crack, perpendicular to the polar axis, are radically different. Moreover, were such a surface to carry a net charge, the two opposite surfaces would carry charges of opposite sign, as would a pyroelectric crystal. In contrast, the hydrogen-bonded bilayers in Fig. 2D are centrosymmetric and thus nonpolar. Subsequently, the opposite faces within the crack have similar structures, with no net charge on each of these two surfaces, although they may carry locally charged groups. Therefore, we anticipate that an effective net charge on the opposite surfaces of cracks along the polar axis can produce an electric field across the fissure strong enough to help orient water molecules within and to yield ice nuclei, which are proton-ordered and polar along its hexagonal axis. However, it is well established

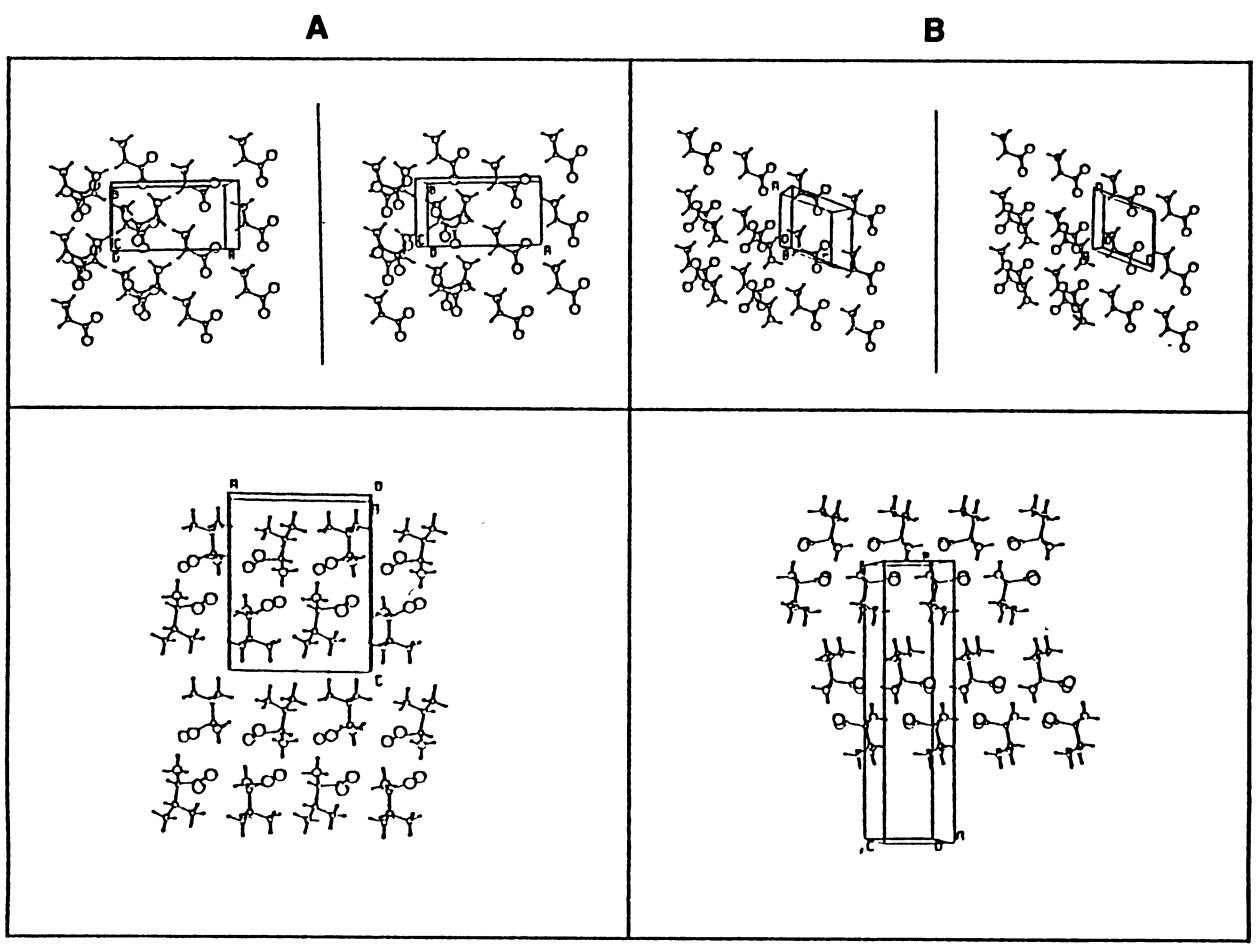

Fig. 1. Comparison of packing arrangements of L-Val (**A**) and D,L-Val (**B**). The upper figures show stereoscopic views of the hydrogen-bonded layers, which omit the isopropyl groups. Note the similarity in the layer structures of L- and D,L-Val. Also shown are several molecules of an upper layer. In L-Val the two layers are related by (pseudo) rotation symmetry about the polar *b* axis (which is in the vertical direction); in D,L-Val the two layers are related by a center of inversion. The lower figures show side views of neighboring hydrogen-bonded bilayers. In L-Val (A) the neighboring bilayers are related by translation. In D,L-Val (B) the neighboring bilayers are related by twofold screw symmetry.

that the crystal structure of hexagonal ice is proton-disordered and thus nonpolar. Nevertheless, we may envisage nucleation of a partially polar proton-ordered ice crystallite within a narrow polar crack, the dimensions of which are much smaller than the observed surface cracks, before growth into the normal mature form (*20*). According to this model, we predicted that for an α-amino acid crystal pair whose racemic and chiral-resolved counterparts have similar structure and morphology but for which the racemate has a polar axis whereas the chiral crystal has no polar axes, the racemate should be the better ice nucleator. Ala and Tyr were found to satisfy these structural conditions.

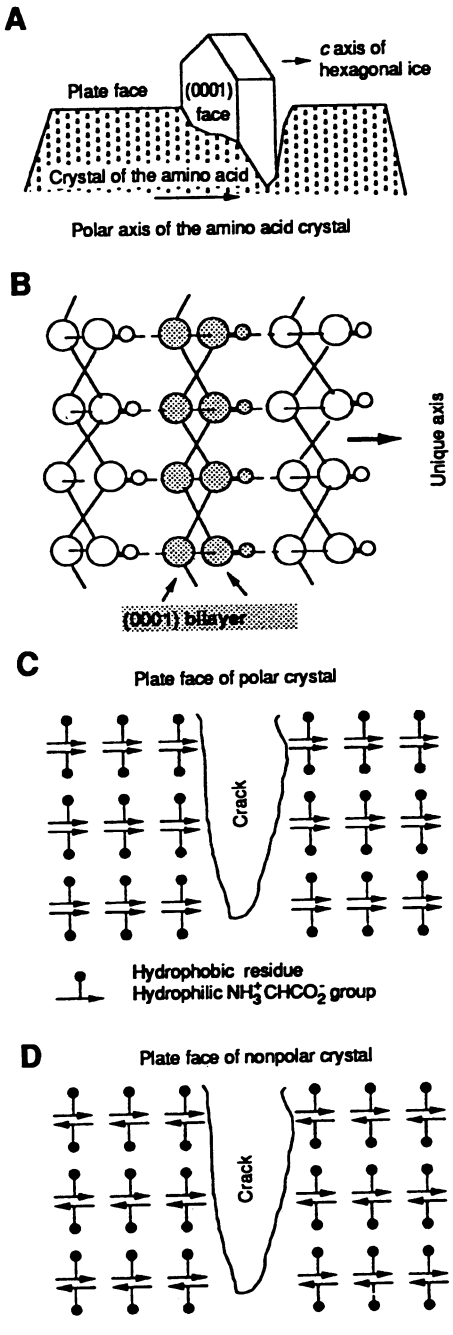

Fig. 2. (**A**) Schematic view of hexagonal ice crystals (exaggerated for clarity) emerging from the plate face of an α-amino acid crystal. (**B**) Molecular packing of a hexagonal ice form in which the O–H···O hydrogen bonds along the unique axis are assumed to be proton-ordered and so the structure is polar along this direction. The three remaining O–H···O bonds per molecule within each (0001) bilayer are assumed to be proton-disordered. (**C**) Schematic view of a polar α-amino acid crystal composed of hydrogen-bonded bilayers. The polar axis is along the horizontal direction. The opposite faces within the crack expose different groups. (**D**) Schematic view of the centrosymmetric α-amino acid crystal. The opposite faces within the crack are equivalent.

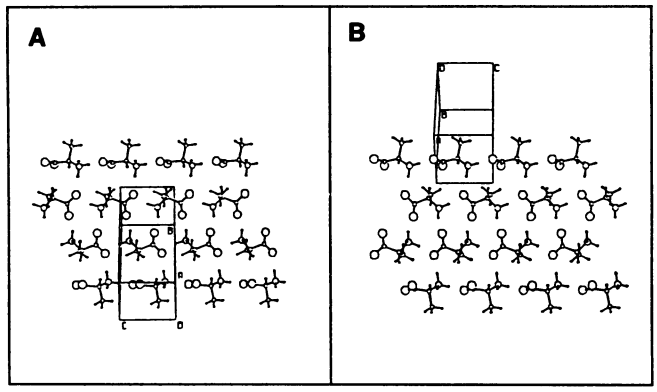

Fig. 3. (**A**) Packing arrangement of L-Ala. (**B**) Packing arrangement of D,L-Ala.

D,L-Ala (*21*) crystallizes in polar space group $Pna2_1$ and L-Ala (*22*) in space group $P2_12_12_1$. The crystal of the racemate contains parallel hydrogen-bonded chains along the polar *c* axis (Fig. 3B). L-Ala (Fig. 3A), which has unit cell axes similar in length to those of D,L-Ala, is built of the same type of hydrogen-bonded chains along the *c* axis as D,L-Ala, but the neighboring isochiral chains are antiparallel. Thus, the crystal has no net dipole moment (*23*). Appropriate [001] needles delineated by four {120} side faces of the racemate were grown from aqueous solution, whereas the [001] needles of the resolved Ala were grown from a 1:1 water-ethanol solution. In both crystals, the {120} faces are hydrophobic because the methyl groups of Ala emerge from them (*24*). Fissures at these faces expose the hydrophilic CO_2^- and NH_3^+ groups. Therefore, these crystals should be comparable to crystals of the hydrophobic α-amino acids listed in Table 1A in their ability to induce ice nucleation.

Racemic (*25*) and chiral-resolved (*26*) Tyr bear the same relation to one another in terms of space group symmetry (Table 1B) and cell dimensions as Ala (*27*). Their crystals proved to be very thin needles, and so bunches of them were used as substrate for the freezing point measurements. We found, in keeping with prediction, that racemic Ala and Tyr are better ice nucleators than their chiral counterparts (Table 1B).

These conclusions are in agreement with calculations of the interaction energy (*28*) between an Ala crystal with a crevice and a polar hexagonal ice-like cluster contained within the crevice for both the L- and the D,L forms. Ala crystals containing about 380 molecules were created in which the crevices with sides approximately parallel to the (001) plane were formed by exclusion of 12 to 20 Ala molecules. The dimensions of these sides were about 17 Å by 15 Å. The width of the crevice was the same for the D,L and L crystals. The crevice walls were separated along the *c* axis by one or two unit cell lengths to permit the intercalation of single or double ice-like (0001) bilayers (see Fig. 2B) containing 14 and 34 water molecules, respectively. In both cases the interaction energy involving D,L-Ala was decidedly lower than the corresponding value for L-Ala (*29*): The resulting energy difference for a single bilayer in a narrow crevice was 0.9 kcal/mol, whereas for the double bilayer in a wider crevice the difference was 1.3 kcal/mol. The contribution of nonbonded interactions to the above difference was very small, and the energy was insensitive to rotation of the ice cluster about its central axis. Thus it is the more favorable electrostatic energy of interaction in the D,L crystal crevice that assists the organization of the water molecules into ice-like aggregates at a temperature higher than in the L crystal (*30*). Calculations performed by Zhu and Robinson on the structure of liquid water between electrically charged plates (*31*) indicate that the water structure close to the plate is substantially different from that in the bulk liquid and that the electric field has a strong alignment effect near the plates.

We propose, on the basis of the results presented here, that an electric field mechanism may be of general applicability for ice nucleation and could also operate in simple systems such as crystals of AgI, which are polar along their hexagonal axis. We may envisage an analogous induction role for

the frost bacterium *Pseudomonas syringae*. Its ice-nucleating ability arises from proteins bearing a sixfold repetition of octapeptide building blocks. As pointed out by Green and Warren (*4*) and Mizuno (*32*), one may construct molecular models with these octapeptides with lattice (but not structure) symmetry to match the hexagonal lattice of ice. In line with the theme of this report, we propose that the helix dipole moment of the octapeptide moiety may play a role for induced freezing in the pockets between helices of polar arrangement.

REFERENCES AND NOTES

1. K. B. Storey and J. M. Storey, *Sci. Am.* **263**, 62 (December 1990).
2. A. L. DeVries, *Philos. Trans. R. Soc. London Ser. B* **304**, 575 (1984).
3. R. E. Feeney, T. S. Burcham, Y. Yeh, *Annu. Rev. Biophys. Biophys. Chem.* **15**, 59 (1986).
4. R. L. Green and G. J. Warren, *Nature* **317**, 645 (1985).
5. S. E. Lindow, *Annu. Rev. Phytopathol.* **21**, 363 (1983).
6. B. Vonnegut, *J. Appl. Phys.* **18**, 593 (1947).
7. M. L. Corrin and J. A. Nelson, *J. Phys. Chem.* **72**, 643 (1968).
8. D. N. Blair, B. L. Davis, A. S. Dennis, *J. Appl. Meteorol.* **12**, 1012 (1973).
9. B. L. David, L. R. Johnson, F. John Moeng, *ibid.* **14**, 891 (1975).
10. M. Gavish, R. Popovitz-Biro, M. Lahav, L. Leiserowitz, *Science* **250**, 973 (1990).
11. D. Jacquemain *et al.*, *J. Am. Chem. Soc.* **113**, 7684 (1991).
12. J.-L. Wang *et al.*, unpublished results.
13. B. A. Power and R. F. Power, *Nature* **194**, 1170 (1962).
14. N. Barthakur and J. Maybank, *ibid.* **200**, 866 (1963).
15. F. P. Parungo and J. P. Lodge, Jr., *J. Atmos. Sci.* **22**, 309 (1965); *ibid.* **24**, 274 (1967).
16. K. Torii and Y. Iitaka, *Acta Crystallogr. Sect. B* **26**, 1317 (1970); M. Mallikarjunan and S. Thyagaraja Rao, *ibid.* **25**, 296 (1969); M. Coll, X. Solans, M. Font-Altaba, J. A. Subirana, *Acta Crystallogr. Sect. C* **42**, 599 (1986); B. di Blasio, C. Pedone, A. Sirigu, *Acta Crystallogr. Sect. B* **31**, 601 (1975), K. Torii and Y. Iitaka, *ibid.* **27**, 2237 (1971); E. Benedetti, C. Pedone, A. Sirigu, *ibid.* **29**, 730 (1973); K. Torii and Y. Iitaka, *ibid.*, p. 2799; A. McL. Mathieson, *Acta Crystallogr.* **5**, 332 (1952); *ibid.* **6**, 399 (1953).
17. I. Weissbuch, F. Frolow, L. Addadi, M. Lahav, L. Leiserowitz, *J. Am. Chem. Soc.* **112**, 7718 (1990).
18. S. Grayer Wolf, theses, Feinberg Graduate School, Weizmann Institute of Science, Rehovot, Israel (1986 and 1990). In crystal structures of chiral-resolved Val, Leu, Ile, and Met, each hydrogen-bonded layer contains two crystallographically independent molecules related by pseudo-translation in a pseudo-centered cell; the actual space group is $P2_1$. The neighboring layers, related by twofold screw symmetry, are interlinked by N–H···O bonds to form a bilayer. The two independent molecules of neighboring layers forming the bilayer are related by pseudo-twofold symmetry to form a hydrogen-bonded pair. In the crystal structures of Norleu and α-amino octanoic acid, the space group is *C*2, so that the cell is truly centered and the molecules forming a hydrogen-bonded pair are related by twofold symmetry.
19. Hexagonal ice has space group $P6_3/mmc$, with cell dimensions $a = b = 4.5$ Å, $c = 7.3$ Å, $\gamma = 120°$; these dimensions are similar to those of β-AgI with space group $P6_3mc$, cell dimensions $a = b = 4.59$ Å, $c = 7.51$ Å, $\gamma = 120°$, but different from those of the α-amino acids. Cell dimensions of some α-amino acids are as follows: D,L-Val, $a = 5.21$ Å, $b = 22.10$ Å, $c = 5.41$ Å, $\beta = 109.2°$; L-Val, $a = 9.71$ Å, $b = 5.27$ Å, $c = 12.06$ Å, $\beta = 90.8°$; D,L-Leu, $a = 14.12$ Å, $b = 5.39$ Å, $c = 5.19$ Å, $\alpha = 111.1°$, $\beta = 97.0°$, $\gamma = 86.4°$; L-Leu, $a = 9.61$ Å, $b = 5.31$ Å, $c = 14.72$ Å, $\beta = 93.8°$; D,L-Met, $a = 9.89$ Å, $b = 4.70$ Å, $c = 16.74$ Å, $\beta = 102.3°$; L-Met, $a = 9.50$ Å, $b = 5.19$ Å, $c = 15.32$ Å, $\beta = 97.7°$.
20. Because the (0001) face of hexagonal ice is a dominant face, it is reasonable that crystals with such morphology would emerge from the fissure even in the absence of the electric field, as was found for the racemic crystals of Table 1A.
21. J. Donohue, *J. Am. Chem. Soc.* **72**, 949 (1950).
22. H. J. Simpson, Jr., and R. E. Marsh, *Acta. Crystallogr.* **20**, 550 (1966).
23. This property is easily understood in terms of the corresponding 222 point group; a vector (or dipole moment) operated on by the three perpendicular twofold rotation axes of the 222 group has a null resultant value. Thus we have a paradoxical situation such that, although $P2_12_12_1$ is a polar space group in which only the principal planes are nonpolar, the crystal has no net dipole moment.
24. Crystals of L-Ala grown from an aqueous solution did not develop [001] needles with dominant {120} faces, but rather {011}.
25. A. Mostad and C. Romming, *Acta Chem. Scand.* **27**, 401 (1973).
26. A. Mostad, H. M. Nissen, C. Romming, *ibid.* **26**, 3819 (1972).
27. The cell dimensions of these amino acids are as follows: L-Ala, $a = 12.26$ Å, $b = 5.93$ Å, $c = 5.79$ Å, D,L-Ala, $a = 12.04$ Å, $b = 6.04$ Å, $c = 5.81$ Å; L-Tyr, $a = 21.11$ Å, $b = 6.91$ Å, $c = 5.82$ Å; D,L-Tyr, $a = 20.81$ Å, $b = 6.81$ Å, $c = 5.90$ Å.
28. We performed atom-atom potential energy calculations using van der Waals' parameters taken from the 6-9 set of A. T. Hagler, E. Huler, and S. Lifson [*J. Am. Chem. Soc.* **96**, 5319 (1974)] and S. Lifson, A. T. Hagler, and P. Dauber [*ibid.* **101**, 5111 (1979)]. The atomic electrostatic moments, that is, atomic charges, dipoles, and quadrupoles, were derived from the experimental deformation electron density of L-Ala, based on the low-temperature (20 K) x-ray diffraction data of R. Destro, R. E. Marsh, and R. Bianchi [*J. Phys. Chem.* **92**, 966 (1988)] and on that of water in the low-temperature (~100 K) structure of cytosine monohydrate [M. Eisenstein, *Acta Crystallogr. Sect. B* **44**, 412 (1988)]. We obtained the deformation electron densities for both structures using the method of F. Hirshfeld [*Acta Crystallogr. Sect. B* **27**, 769 (1971); *Isr. J. Chem.* **16**, 226 (1977)] and partitioned them to yield the atomic moments according to the stockholder recipe of F. L. Hirshfeld [*Theor. Chim. Acta* **44**, 129 (1977)]. The net charges on the carboxylate CO_2^- and amino NH_3^+ groups of Ala were found to be about 0.6 electron unit.
29. The average calculated interaction energy per water molecule within the single ice-like (0001) bilayer was −3.8 kcal/mol for D,L-Ala and −2.9 kcal/mol for L-Ala; the corresponding values for the double layer were −4.0 and −2.7 kcal/mol, respectively. The interaction is favorable in both cases, but more so for the D,L form, in agreement with experiment.
30. The entropy difference between ice proton-ordered along the hexagonal axis and completely proton-disordered ice in terms of energy is about 0.1 kcal/mol at 0°C.
31. S.-B. Zhu and G. W. Robinson, *J. Chem. Phys.* **94**, 1403 (1991).
32. H. Mizuno, *Proteins* **5**, 47 (1989).

33. This work was supported by the Minerva Foundation, the U S.–Israel Binational Foundation, and the Petroleum Research Fund of the American Chemical Society. M.G. was the recipient of a postdoctoral fellowship from the Feinberg Graduate School of the Weizmann Institute of Science. Dedicated in memory of F L. Hirshfeld.

19 November 1991; accepted 20 February 1992

Metallo-Carbohedrenes: Formation of Multicage Structures

S. Wei, B. C. Guo, J. Purnell, S. Buzza, A. W. Castleman, Jr.*

An unusual structural growth pattern has been found in the system of Zr_mC_n, in which multicage structures are formed. The experimental evidence shows that the first cage closes at Zr_8C_{12}. Surprisingly, subsequent cluster growth does not lead to the enlargement of the cage size as it usually does in the case of pure carbon clusters and water clusters, for example. Rather, multicage structures are developed, that is, a double cage at $Zr_{13}C_{22}$ and $Zr_{14}C_{21/23}$, a triple cage at $Zr_{18}C_{29}$, and a quadruple cage at $Zr_{22}C_{35}$. This feature distinguishes the class of metallo-carbohedrenes from the regular doped fullerenes.

Recent studies have revealed the existence of a general class of materials, referred to as metallo-carbohedrenes, which have shown prominent species corresponding to the composition M_8C_{12}, M being Ti, V, Zr, and Hf (*1*, *2*). A cage-like pentagonal dodecahedron structure was proposed to account for their exceptional stability. We report further evidence supporting this cage-like structure, namely that cluster growth proceeds through the formation of multicage structures. Our new studies of clusters comprised of Zr_mC_n show that the first complete cage (Fig. 1A) closes at Zr_8C_{12}; subsequent attachment of metal-carbon units leads to the completion of double-cage structures (Fig. 1B) formed at $Zr_{13}C_{22}$ and $Zr_{14}C_{21/23}$, whereas a triple cage (Fig. 1C) is developed at $Zr_{18}C_{29}$ and a quadruple cage at $Zr_{22}C_{35}$ (Fig. 1D).

The apparatus used in these experiments is a reflectron time-of-flight (TOF) mass spectrometer coupled with a laser vaporization source. Metal-carbon clusters are produced through plasma reactions between metals and various small hydrocarbons (*1*, *3*), and the neutral clusters formed into a molecular beam are then ionized by an

Department of Chemistry, The Pennsylvania State University, University Park, PA 16802.

*To whom correspondence should be addressed.